

Development of dimensionless P-I diagram for curved SCS sandwich shell subjected to uniformly distributed blast pressure

Yonghui WANG^{a,b*}, Ximei ZHAI^{a,b}

^a Key Lab of Structures Dynamic Behavior and Control of the Ministry of Education, Harbin Institute of Technology, Harbin 150090, China

^b Key Lab of Smart Prevention and Mitigation of Civil Engineering Disasters of the Ministry of Industry and Information Technology, Harbin Institute of Technology, Harbin 150090, China

*Corresponding author: E-mail: wangyonghui@hit.edu.cn

© Higher Education Press and Springer-Verlag GmbH Germany, part of Springer Nature 2019

ABSTRACT The curved steel-concrete-steel (SCS) sandwich shell was recently proposed to resist blast loading and it showed better blast resistant performance as compared to flat SCS sandwich shell via developing compressive force along the shell. In this paper, a dimensionless Pressure-Impulse (P-I) diagram was constructed as a convenient tool to predict the damage level of curved SCS sandwich shell subjected to uniformly distributed blast loading. The curved SCS sandwich shell was equivalent to a single-degree-of-freedom (SDOF) system and the equation of motion was established by employing the Lagrange's equation. To construct the dimensionless P-I diagram, the energy balance method was utilized to yield the pressure and impulse asymptotes and the responses in the dynamic response regime were obtained via employing the SDOF method. Then, the finite element method was employed to validate the developed dimensionless P-I diagram. Finally, the procedures of using the constructed dimensionless P-I diagram to quickly conduct the blast resistant design of curved SCS sandwich shell were presented.

KEYWORDS blast loading, curved steel-concrete-steel sandwich shell, Pressure-Impulse diagram, single-degree-of-freedom method, finite element analysis

1 Introduction

Steel-concrete-steel (SCS) sandwich shell consists of a concrete core connected to two external steel face plates using mechanical shear connectors. The composite action of a SCS sandwich structure is achieved through shear connectors to bond the two face plates to the concrete core. Several types of shear connectors have been developed, including headed shear studs [1], angle shear connectors [2], Bi-steel [3], and interlocked J-hook connectors [4–6]. The impact and blast resistant performances of flat SCS sandwich shells were extensively studied [6–13] and they showed high performance in resisting impact and blast loading due to high ductility, spalling protection, buckling resistance, and energy absorption. Recently, the curved

SCS sandwich shell was appealing in resisting blast loading, since the curved shell normally performed better than the flat shell under blast loading via developing compressive force along the shell [14]. Therefore, the curved SCS sandwich shell has high potential application as blast resistant wall, as illustrated in Fig. 1. Up to date, several studies on the punching resistance of curved SCS sandwich shell under concentrated load were conducted [15–20]. However, minimal reported works on the curved SCS sandwich shell under blast loading were found in Ref. [14] and the blast resistant design approach of such structure was also not available. Hence, the aim of this work is to develop a dimensionless Pressure-Impulse (P-I) diagram for the curved SCS sandwich shell under uniformly distributed blast loading, which can be employed as a convenient tool to predict the damage level of such structure.

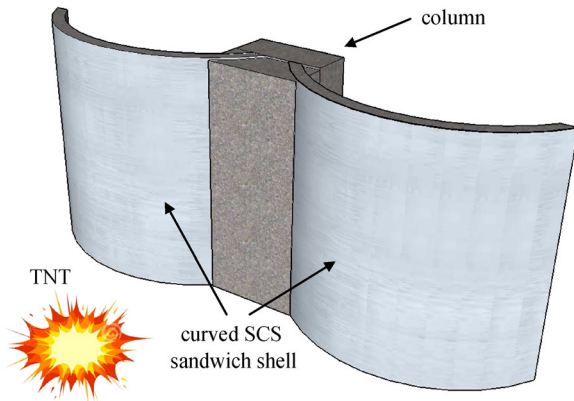


Fig. 1 Curved SCS sandwich shell as blast resistant wall.

The equivalent single-degree-of-freedom (SDOF) method was widely used as a simple alternative to predict the dynamic response of continuous member subjected to blast loading [21–28]. This method was also adopted by many design guidelines [29–31] to evaluate the blast induced damage level of a structure, since it could capture the global structural response with reasonable accuracy. Another simple method to predict the damage level of a structure under blast loading is P-I diagram, which is an iso-damage curve for a particular structural member loaded with a particular blast load history [32]. There are mainly two methods to construct P-I diagrams, i.e., SDOF method [33–37] and finite element (FE) method [38,39]. As for the SDOF method, the pressure and impulse asymptotes of a P-I diagram can be directly expressed as formulae in terms of structural parameters, such as stiffness, mass, and allowable maximum displacement, etc. Support rotation or ductility ratio was usually adopted by the design guidelines to gauge the damage level of a structure [29–31] and they could be directly obtained via employing the SDOF method. Hence, support rotation or ductility ratio was normally adopted as the damage level indicator for the P-I diagram generated via employing the SDOF method. This is reasonable for the structural members like beams and slabs but not appropriate for columns whose failure is usually governed by residual axial strength. Therefore, the FE method with easier output of residual axial strength is preferred to construct the P-I diagram of columns. Shi et al. [38] and Mutalib and Hao [39] utilized the FE method to generate the P-I diagram for Reinforced Concrete (RC) columns and Fiber-Reinforced Polymer (FRP) strengthened RC columns, respectively. In their studies, the residual axial strength was applied as the damage level indicator, which was more representative than support rotation or ductility. Parametric studies and curve-fitting might be required to establish the relationship between pressure/impulse asymptotes and structural parameters.

This paper starts with a description on the establishment of FE model of curved SCS sandwich shell under blast loading and its verifications with test results, followed by

the construction of SDOF model and dimensionless P-I diagram. Then, the developed dimensionless P-I diagram was validated with the FE results. Finally, the procedures of using the dimensionless P-I diagram to conduct the blast resistant design of curved SCS sandwich shell were presented.

2 FE model establishment and verification

The numerical method has been successfully applied for recent decades in modeling of curved shells [40,41], sandwich structures [42], and concrete [43–45]. In this work, the explicit code in LS-DYNA was employed to simulate the dynamic responses of curved SCS sandwich shells under blast loading and the accuracies of the established FE models were verified with the available experimental results. The established FE models in this section would be used to validate the developed dimensionless P-I diagram in Section 4.

2.1 FE model of curved SCS sandwich shell

In this study, quarter FE model of curved SCS sandwich shell was established in Fig. 2 due to the symmetry of geometry and applied blast loading. The nodes on the end plate were restricted from translation to simulate the fixed boundary condition. The steel plates were meshed using S/R Hughes-Liu shell element and eight-node solid element with reduced integration in combination with hourglass control was employed for the concrete core. The soft constraint-based contact approach [46] was adopted to simulate the contact between steel plates and concrete core.

Traditional detailed FE modeling of SCS sandwich shell was employing solid elements for steel plates, concrete core and shear connectors [47,48]. This modeling approach inevitably resulted in finer meshes at shear connectors and steel plates adjacent to shear connectors [47], which led to smaller time step and longer calculating time. Anandavalli et al. [8] employed more uniform meshing approach, i.e., using shell and link elements for the steel plates and shear connectors, respectively. In this study, a simplified approach that employed Hughes-Liu beam elements [46] for shear connectors and assumed perfect bond between concrete core and shear connectors was adopted. This approach was also used to model reinforced concrete structures against blast loading and the predictions were proven to be acceptable [49,50]. Figure 3 illustrates the modeling of connection between steel plates and shear connectors. The circular rigid panel with the same diameter of shear connector is attached to the shear connector through shared node and meanwhile tied to the steel plate. This connection modeling approach can avoid stress concentration at the steel plate introduced by directly sharing the node between the shear connector and steel plate. The geometry of

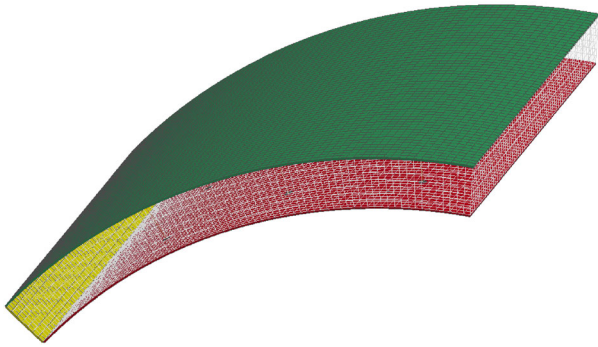


Fig. 2 Quarter FE model of curved SCS sandwich shell.

curved SCS sandwich shell used to validate the dimensionless P-I diagram is given in Table 1 and the uniformly distributed blast loading was applied to the surface of outer steel plate.

The Continuous Surface Cap Model (CSCM) in LS-DYNA [46] was adopted to model the behavior of concrete. This material model was developed by US Federal Highway Administration to simulate the concrete-like material subjected to high rate loading, like impact and blast [51,52]. The detailed description of CSCM model, including failure surface, flow rule and strain rate effect treatment, etc., can be found in Ref. [51]. This material model can generate the default parameters for the normal weight concrete by only inputting the unconfined compressive strength. The main parameters of concrete used in this analysis are given in Table 2. As for the simulation of steel, the Piecewise Linear Plasticity material model in LS-DYNA [46] was employed. The material properties of steel were obtained from the tensile coupon test and the input

true stress-effective plastic strain curve is shown in Fig. 4. In this material model, the Cowper-Symonds model [53] is adopted to scale the yield stress as

$$\sigma_y(\dot{\epsilon}_{eff}^p, \epsilon_{eff}^p) = \sigma_y(\epsilon_{eff}^p) \left[1 + \left(\frac{\dot{\epsilon}_{eff}^p}{C} \right)^{1/P} \right], \quad (1)$$

where $\sigma_y(\epsilon_{eff}^p)$ is the yielding stress without considering strain rate effects, $\dot{\epsilon}_{eff}^p$ is the effective plastic strain rate, C and P are the strain rate parameters. In this study, the strain rate parameters C and P are 40.4 and 5 for steel plate [54].

2.2 FE model verification

Since there is no experimental data on curved SCS sandwich panel subjected to blast loading available in the open literature, the field blast test conducted by Liew and Wang [11] and Kang et al. [55] on the flat SCS sandwich shell, which has similar configuration of curved SCS sandwich shell, was adopted to validate the FE model of curved SCS sandwich shell and the comparisons between the FE and experimental results were presented in Ref. [9] and summarized in Figs. 5 and 6. The measured permanent deformation from field blast test shows good agreement with the FE prediction, as seen in Fig. 5. In addition, the failure mode of flat SCS sandwich shell from FE analyses is also compared with that from field blast test in Fig. 6. Both the FE and test results show the bending failure mode at mid-span and with sign of shear deformation near the top end. From above comparisons, the established FE model of SCS sandwich shell under blast loading is considered to be reliable in terms of the element meshing and formulation as well as the input material properties of concrete and steel. To verify the

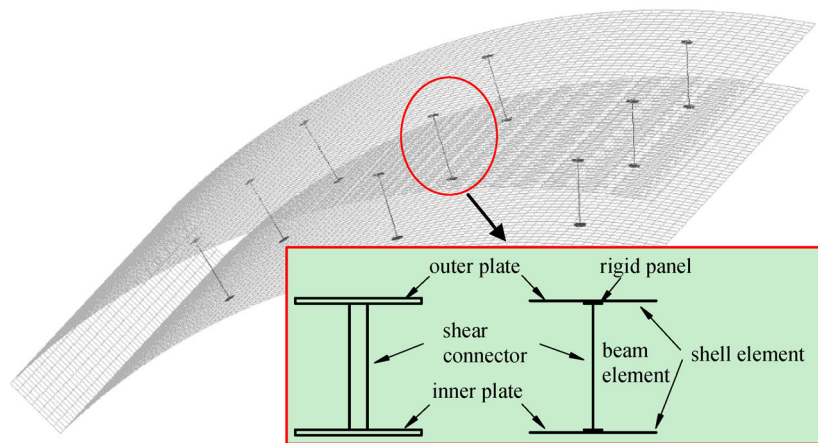


Fig. 3 Simplified FE model of shear connectors.

Table 1 Geometry of curved SCS sandwich shell (unit: mm)

span	width	rise height	steel plate thickness	concrete depth	shear connector diameter	shear connector spacing
1200	1200	300	3	70	10	200

Table 2 Material properties of concrete in FE analysis

density (kg/m ³)	compressive strength (MPa)	shear modulus (GPa)	bulk modulus (GPa)
2310	35	12.06	13.21

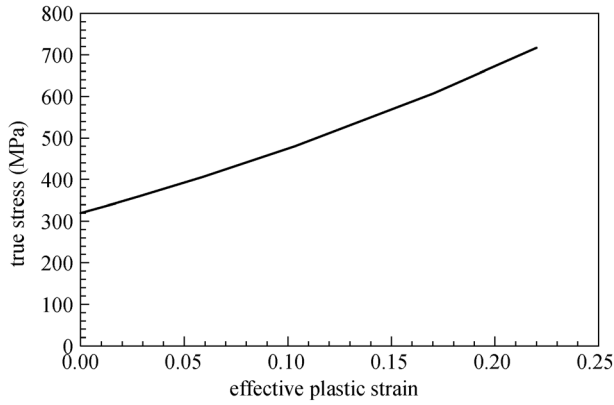


Fig. 4 True stress-effective plastic strain curve for mild steel.

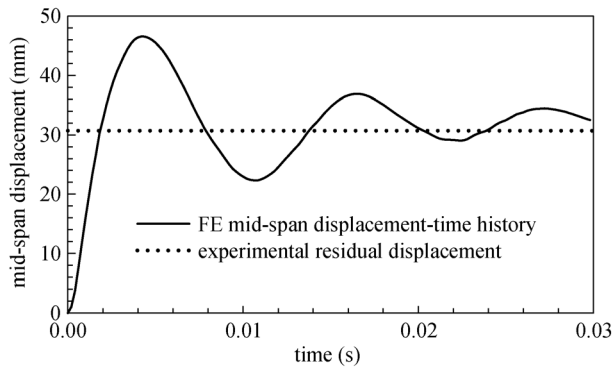


Fig. 5 Comparison of FE predictions with test results.

proposed FE modeling approach of shear connectors, the static test on SCS sandwich beam with shear connectors friction-welded to the steel plates [56] was employed. The same material models, element formulations and mesh size in Section 2.1 were used herein. The geometry of the SCS beam is given in Fig. 7 and the material properties are

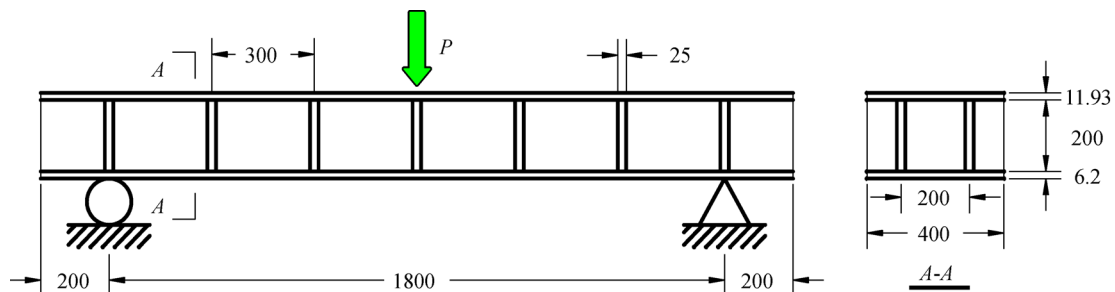


Fig. 7 Details of SCS sandwich beam (unit: mm).

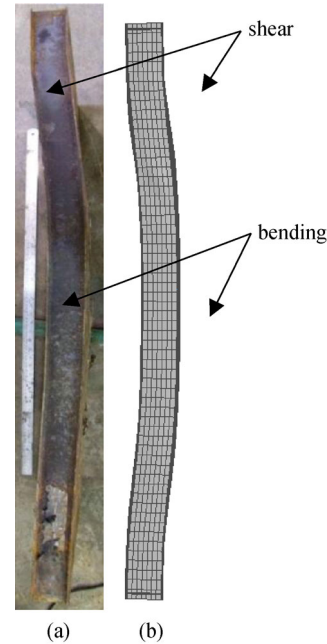


Fig. 6 Comparison of failure modes: (a) test observation and (b) FE prediction.

given in Table 3. The load-displacement response of the SCS sandwich beam under concentrated load from the test [56] is compared with the FE simulation results with different modeling approaches of shear connectors, as shown in Fig. 8. All the three modeling approaches can yield similar ultimate strength. However, the discrepancy is observed at initial loading stage, i.e., ‘solid elements modeling approach’ by Foundoukos and Chapman [47] shows stiffer response as compared to the test results, and ‘shell and link modeling approach’ by Anandavalli et al. [8] shows softer response. It is also noted that the proposed ‘shell and beam modeling approach’ shows better agreement with the test results, which validates the proposed FE modeling approach of shear connectors. From above comparisons, the established FE model is able to reasonably capture the response of curved SCS sandwich shell under blast loading and can be employed to validate the generated dimensionless P-I diagram in the following sections.

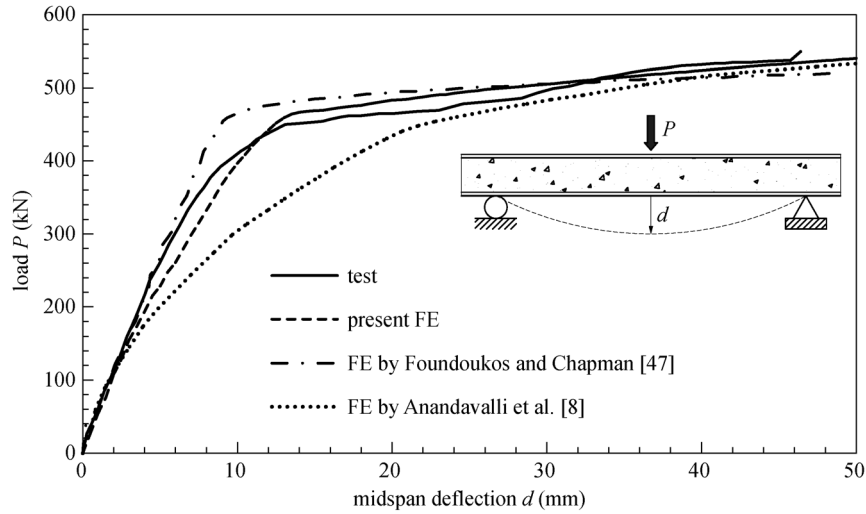


Fig. 8 Load-displacement response of SCS sandwich beam.

Table 3 Material properties of steel and concrete in Ref. [50]

f_{yP} (MPa)	f_{uP} (MPa)	f_{yB} (MPa)	f_{uB} (MPa)	f_{cu} (MPa)
384	507	541	566	58

Note: f_{yP} , f_{uP} are yield strength and ultimate strength of tension steel plate, respectively; f_{yB} , f_{uB} are yield strength and ultimate strength of shear connector, respectively; f_{cu} is cube strength of concrete.

3 SDOF system of curved SCS sandwich shell

The SDOF method was adopted in this study to obtain the blast responses of curved SCS sandwich shells, based on which, the dimensionless P-I diagram was constructed. The curved SCS sandwich shell under uniformly distributed blast loading can be equivalent to a SDOF system and the procedures to establish the equation of motion (EOM) are described as follows: 1) assume a reasonable deflection shape function, which can be obtained by applying the uniformly distributed loading on the structure in a static manner [21]; 2) establish the relationship between strain and mid-span displacement; 3) derive the internal energy, kinetic energy of curved SCS sandwich shell in terms of mid-span displacement and velocity, respectively, and substitute them together with the potential energy of applied blast loading into the Lagrange’s equation of motion.

3.1 Deflection shape function

For a one-way supported curved SCS sandwich shell under uniformly distributed loading shown in Fig. 9, it can be simplified as an arch, since the displacement in the radial direction is predominant and its value along the width direction is almost same. Hence, the deflection shape function of the arch under uniform line load can be adopted to represent the deflection shape function of curved SCS

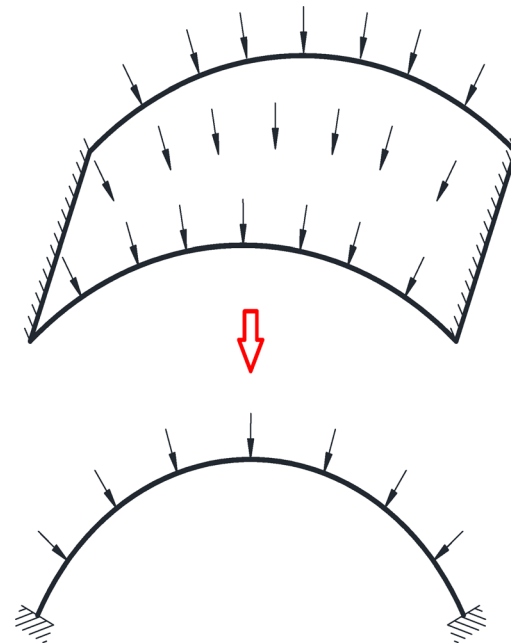


Fig. 9 Simplification of curved shell to an arch.

sandwich shell under uniformly distributed loading. As shown in Fig. 10 for the elastic arch under uniform line load, q , in the radial direction, the radial displacement (inwardly positive), $w(\theta)$, and tangential displacement, $v(\theta)$, are given as follows [57]:

$$w(\theta) = \frac{qR^4}{EI} \left\{ \left[\left(\frac{1+\bar{I}}{2} \right) \theta \sin\theta \right] C_1 - \bar{I}C_2 + (\bar{I}\cos\theta)C_3 + \bar{I} \right\}, \tag{2}$$

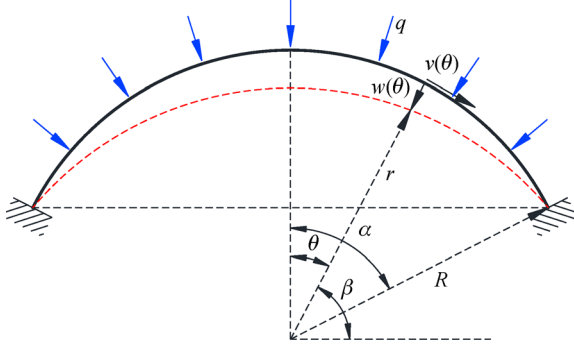


Fig. 10 Geometry of arch.

$$v(\theta) = \frac{qR^4}{EI} \left\{ [(1-\bar{I})\sin\theta - (1+\bar{I})\theta\cos\theta] \frac{C_1}{2} - (\bar{I}\theta)C_2 + (\bar{I}\sin\theta)C_3 \right\}, \quad (3)$$

where q is uniform line load, R is radius of arch, E is Young's modulus, I is area's second moment, $\bar{I} = h^2/12R^2$ (h is thickness of arch), C_1 , C_2 , and C_3 are unknown constants and can be determined by applying boundary conditions. For an arch with fixed ends, the following boundary conditions are applied:

$$w(\alpha) = 0, v(\alpha) = 0, \left. \frac{dw}{d\theta} \right|_{\theta=\alpha} = 0. \quad (4)$$

Then, the constants C_1 , C_2 and C_3 can be determined by substituting the boundary conditions in Eq. (4) into Eqs. (2) and (3) as follows:

$$C_1 = \frac{\bar{I}\alpha}{\sin\alpha - \frac{1+\bar{I}}{2}\alpha\left(\frac{\alpha}{\sin\alpha} + \cos\alpha\right)}, \quad (5)$$

$$C_2 = \frac{\sin\alpha}{\sin\alpha - \frac{1+\bar{I}}{2}\alpha\left(\frac{\alpha}{\sin\alpha} + \cos\alpha\right)}, \quad (6)$$

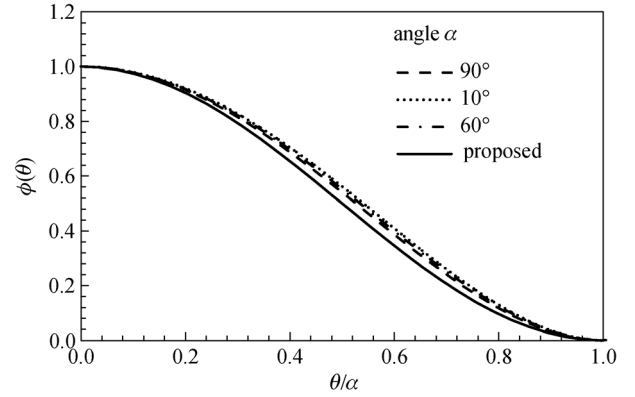
$$C_3 = \frac{\frac{1+\bar{I}}{2}\alpha(1 + \alpha\cot\alpha)}{\sin\alpha - \frac{1+\bar{I}}{2}\alpha\left(\frac{\alpha}{\sin\alpha} + \cos\alpha\right)}. \quad (7)$$

The deflection shape function in the radial direction, $\phi(\theta)$, can be determined via dividing the radial displacement, $w(\theta)$, by the mid-span displacement of the arch, $w(0)$, i.e.,

$$\phi(\theta) = \frac{\sin\alpha \cdot \theta \cdot \sin\theta + (\sin\alpha + \alpha \cdot \cos\alpha) \cdot \cos\theta - \alpha - \sin\alpha \cdot \cos\alpha}{(1 - \cos\alpha)(\sin\alpha - \alpha)}. \quad (8)$$

It is noted in Eq. (8) that the radial deflection shape function varies with angle α , which is also illustrated in Fig. 11. To simplify the calculations of axial strain, internal energy, kinetic energy and potential energy in the following sections, a deflection shape function without the variable of angle α in Eq. (9) is proposed considering the minimal effect on the deflection shape function induced by the variation of angle α from 10° to 90° . It was also noted by Baker et al. [58] that the effect of deflection shape function on the structure's response under blast loading was not significant if the adopted deflection shape functions were in accordance with the boundary conditions. Hence, the simplified deflection shape function in Eq. (9), showing only minimal difference with the original ones, is adopted in the following calculations.

$$\phi(\theta) = \frac{1}{2} \left[1 + \cos\left(\frac{\pi\theta}{\alpha}\right) \right]. \quad (9)$$

Fig. 11 Deflection shape with varying angle α .

3.2 Strain-displacement relationship

Establishing the relationship between strain and mid-span displacement is a primary to derive the internal energy in terms of mid-span displacement. In this study, the uniformly distributed compressive strain on the entire arch is assumed in order to provide a simpler close-form solution of internal energy and arithmetic expression of dimensionless P-I diagram. In addition, the geometry requirements of arch are also specified in this section to bring down the errors induced by this assumption.

3.2.1 Strain calculation

By adopting the simplified deflection shape function in Eq. (9), the radial displacement of an arch can be expressed as

$$w(\theta) = \frac{1}{2} \left[1 + \cos\left(\frac{\pi\theta}{\alpha}\right) \right] w_m, \quad (10)$$

where w_m is the mid-span displacement. According to Fig. 10, the developed length of arch can be determined as

$$L_d = \int_{\pi/2-\alpha}^{\pi/2} \sqrt{r^2 + r'^2} d\beta, \quad (11)$$

where $r = R - \frac{1}{2} \left\{ 1 + \cos \left[\frac{\pi}{\alpha} \left(\frac{\pi}{2} - \beta \right) \right] \right\} w_m$ is radius of arch after deformation and $r' = \frac{dr}{d\beta}$. Since it is difficult to obtain the close-form solution of developed length, L_d , from Eq. (11), the following approximation is adopted to derive the developed length of arch as

$$\begin{aligned} L_d &\approx \int_{\pi/2-\alpha}^{\pi/2} \left(\frac{r'^2}{2R} + r \right) d\beta \\ &= R\alpha \left(\frac{1}{4} B_1^2 B_2^2 + 1 - B_1 \right), \end{aligned} \quad (12)$$

where $B_1 = w_m/2R$, $B_2 = \pi^2/2\alpha$. By adopting the assumption that compressive strain is uniformly distributed, the axial strain induced by shortening of arch, ε_c , can be determined as

$$\varepsilon_c = \frac{L_o - L_d}{L_o} = \frac{w_m}{2R} - \frac{1}{16} \left(\frac{w_m \pi}{R\alpha} \right)^2, \quad (13)$$

positive in compression,

where $L_o = R\alpha$ is original length of arch.

3.2.2 Geometry requirements

In reality, the axial strain induced by shortening of arch, ε_c , is not uniformly distributed. Hence, the difference between the maximum and minimum axial strain along the arch needs to be limited to an acceptable value to bring down the errors induced by the assumption. The axial stress resultant of arch can be written as

$$N(\theta) = \frac{EA}{R} \left(\frac{dv(\theta)}{d\theta} - w(\theta) \right), \quad (14)$$

where A is cross-section area of arch [57]. Then, substituting Eqs. (2) and (3) into Eq. (14) leads to

$$N(\theta) = -\frac{qR^3 A \bar{I}}{I} (1 + C_1 \cos\theta). \quad (15)$$

Since the first term in Eq. (15) is only related to the arch's geometry and applied load, the axial strain, ε_c , can be written as

$$\varepsilon_c(\theta) = \bar{\varepsilon} (1 + C_1 \cos\theta), \quad (16)$$

where $\bar{\varepsilon}$ is a function of applied load, geometry, and material properties of arch. It is noted that the axial strain varies along the arch, ranging from $\bar{\varepsilon}(1 + C_1 \cos\alpha)$ at end

to $\bar{\varepsilon}(1 + C_1)$ at mid-span. Hence, the induced strain error, er_ε , can be determined as

$$er_\varepsilon = \left| \frac{\varepsilon_{\max} - \varepsilon_{\min}}{\varepsilon_{\min}} \right| = \left| \frac{C_1(\cos\alpha - 1)}{1 + C_1} \right|, \quad (17)$$

where ε_{\max} and ε_{\min} are the maximum and minimum axial strain along the arch, respectively. It is noted that er_ε is a function of α and h/R and therefore the er_ε in terms of α and h/R are plotted in Fig. 12 to facilitate the selection of acceptable geometry of arch (i.e., the arch with suitable α and h/R satisfying the allowable strain error). It is noted in Fig. 12 that both increasing angle α and decreasing h/R lead to the decrease of strain error.

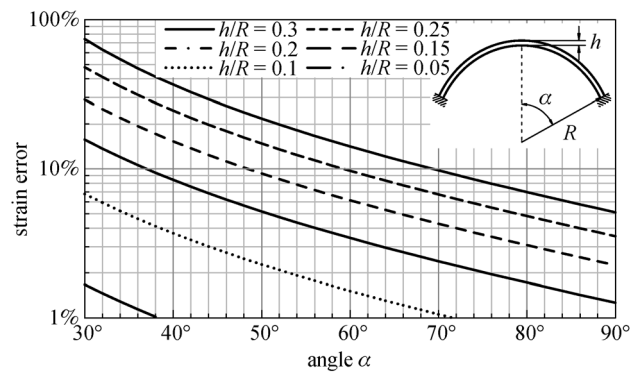


Fig. 12 Effect of α and h/R on the strain error.

Since the compressive strength of concrete is much higher than tensile strength, the continuous compression of arch subjected to blast loading is preferred. Therefore, it is needed to ensure the monotonic increase of axial strain with increasing mid-span displacement before the arch reaching maximum allowable deformation, which leads to the following relationship:

$$\frac{w_{\max}}{R} \leq 4 \left(\frac{\alpha}{\pi} \right)^2, \quad (18)$$

where w_{\max} is the allowable maximum mid-span displacement of arch.

In this calculation, only the axial strain induced by shortening of arch, ε_c , is considered and the axial strain induced by bending, ε_b , is neglected. Similarly, a geometry limit needs to be provided to ensure the resultant axial stress of ε_c and ε_b is in compression on the entire arch. According to Fig. 10, the curvature of arch with thickness of h can be calculated as:

$$k_c(\beta) = \frac{|r^2 + 2r'^2 - rr'|}{(r^2 + r'^2)^{3/2}} = \frac{1}{R} f_1(w_m/R, \alpha, \beta), \quad (19)$$

where $f_1(w_m/R, \alpha, \beta)$ is a function with w_m/R , α , and β as independent variables. Then, the axial strain induced by bending at the outer layer of arch is

$$\varepsilon_b = \frac{h}{2}\Delta k_c = \frac{h}{2R}f_2(w_m/R, \alpha, \beta). \quad (20)$$

It is noted that the maximum axial strain induced by bending, $\varepsilon_{b, \max}$, along the arch locates at the fixed end (i.e., $\beta = \pi/2 - \alpha$) and therefore $\varepsilon_{b, \max}$ can be expressed as a function with w_m/R and α as independent variables, i.e.,

$$\varepsilon_{b, \max} = \frac{h}{2}\Delta k_c = \frac{h}{2R}f_3(w_m/R, \alpha). \quad (21)$$

The requirement of no tensile axial strain on the arch leads to

$$\left| \frac{\varepsilon_{b, \max}}{\varepsilon_c} \right| = \frac{h}{2R}f_4(w_m/R, \alpha) \leq 1. \quad (22)$$

It is noted that $f_4(w_m/R, \alpha)$ shows increase with increasing w_m/R . Hence, the allowable maximum mid-span displacement, w_{\max} , is used to replace w_m in Eq. (22) and this can ensure no tensile axial strain on the arch with mid-span displacement less than w_{\max} . For the curved SCS sandwich shell studied in this paper, the ultimate strain of concrete, ε_u , can be chosen as a failure threshold of curved SCS sandwich shell under blast loading. From Eq. (13), the w_m/R corresponding to ε_u can be determined as

$$\frac{w_{\max}}{R} = 4 \left(\frac{\alpha}{\pi} \right)^2 \left[1 - \sqrt{1 - \left(\frac{\pi}{\alpha} \right)^2 \varepsilon_u} \right]. \quad (23)$$

Substituting Eq. (23) into Eq. (22) and setting $\varepsilon_u = 0.0035$ (with concrete grade no higher than C50/60) [59] leads to the allowable maximum ratio of thickness over radius, $(h/R)_{\max}$, with only α as the independent variable. By utilizing curve fitting method, the expression of $(h/R)_{\max}$ in terms of angle α can be obtained in Eq. (24) and the fitted curve is shown in Fig. 13.

$$\frac{h}{R} \leq \left(\frac{h}{R} \right)_{\max} = (8.925\alpha^2 - 324.9\alpha + 7308) \times 10^{-5}. (\alpha \text{ in } ^\circ) \quad (24)$$

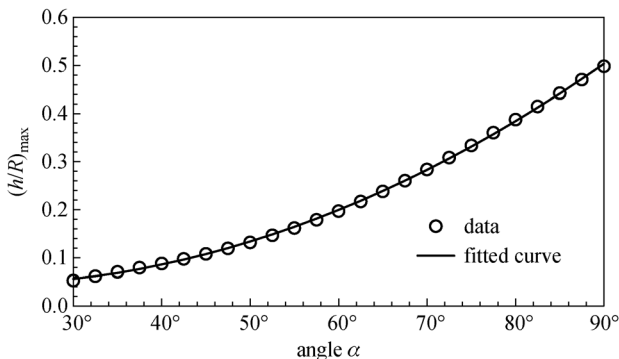


Fig. 13 Relationship between $(h/R)_{\max}$ and angle α .

3.3 Equation of motion

As for the curved SCS sandwich shell with the geometry shown in Fig. 14 subjected to uniformly distributed blast loading, the equation of motion can be formulated in Eq. (25) by applying the Lagrange's equation.

$$\frac{d}{dt} \left(\frac{dK}{d\dot{w}_m} \right) + \frac{d(U + V)}{dw_m} = 0, \quad (25)$$

where K is kinetic energy, U is internal energy, V is potential energy and w_m is mid-span displacement. The kinetic energy of curved SCS sandwich shell can be calculated as

$$K = \frac{1}{2} \int_0^\alpha m [\phi(\theta) \dot{w}_m]^2 d\theta, \quad (26)$$

where m is mass per unit radian of curved SCS sandwich shell and given in Eq. (27), and \dot{w}_m is the velocity at mid-span and can be obtained by differentiating the mid-span displacement, w_m , with respect to time, t .

$$m = \left[\frac{1}{2} \rho_c (r_{out}^2 - r_{in}^2) + \rho_s (t_{in} r_{inm} + t_{out} r_{outm}) \right] W_d, \quad (27)$$

where ρ_c and ρ_s are densities of concrete and steel, respectively, W_d is width of curved SCS sandwich shell and other geometric parameters can be found in Fig. 14.

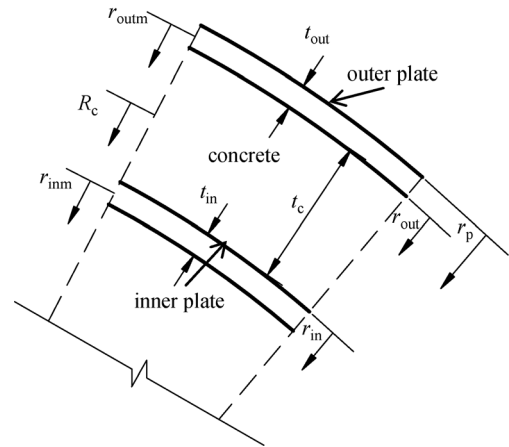


Fig. 14 Geometry of curved SCS sandwich shell.

By adopting the assumption on axial strain in Section 3.2, i.e., the axial strain of concrete, ε_c , is uniformly distributed on the entire concrete core, the differential of internal energy of concrete core, U_c , with respect to mid-span displacement, w_m , can be formulated as

$$\frac{dU_c}{dw_m} = V_c \frac{du_c}{d\varepsilon_c} \frac{d\varepsilon_c}{dw_m}, \quad (28)$$

where $V_c = 1/2(r_{out}^2 - r_{in}^2)W_d$ is volume of concrete core and u_c is internal energy per unit volume of concrete core.

The differential of u_c with respect to ε_c can be determined as

$$\frac{du_c}{d\varepsilon_c} = \sigma_c(\varepsilon_c), \quad (29)$$

where $\sigma_c(\varepsilon)$ specifies the relationship between compressive stress and strain of concrete and can be expressed in Eq. (30) from Eurocode 2 [59].

$$\sigma_c(\varepsilon_c) = \frac{k\varepsilon_c/\varepsilon_o - (\varepsilon_c/\varepsilon_o)^2}{1 + (k-2)\varepsilon_c/\varepsilon_o} f_{cm}, \text{ for } |\varepsilon| < |\varepsilon_u|, \quad (30)$$

where $k, f_{cm}, \varepsilon_o,$ and ε_u are constants for specified concrete grade and can be found in Eurocode 2. From Eq. (13), the differential of ε_c with respect to w_m can be obtained as

$$\frac{d\varepsilon_c}{dw_m} = \frac{1}{2R_c} - \frac{w_m\pi^2}{8R_c^2\alpha^2}, \quad (31)$$

where R_c is radius at the middle layer of concrete core, as shown in Fig. 14.

Similar to the calculation of dU_c/dw_m , the differential of internal energy of inner and outer steel plate with respect to mid-span displacement (dU_{si}/dw_m and dU_{so}/dw_m) can be calculated as well. Herein, the elastic-plastic-hardening constitutive model in Eq. (32) is adopted to determine the stress-strain relationship of steel.

$$\sigma_s(\varepsilon_s) = \begin{cases} E_s\varepsilon_s, & \varepsilon_s \leq \varepsilon_y, \\ E_s\varepsilon_y + \alpha_E E_s(\varepsilon_s - \varepsilon_y), & \varepsilon_s > \varepsilon_y, \end{cases} \quad (32)$$

where $E_s, \varepsilon_y, \alpha_E$ are Young's modulus, yield strain, and hardening coefficient of steel. Hence, the differential of internal energy of curved SCS sandwich shell with respect to mid-span displacement, dU/dw_m , can be obtained by summing the terms of concrete core, inner and outer steel plate as

$$\frac{dU}{dw_m} = \frac{dU_c}{dw_m} + \frac{dU_{si}}{dw_m} + \frac{dU_{so}}{dw_m}, \quad (33)$$

where $U_c, U_{si},$ and U_{so} are internal energy of concrete core, inner, and outer steel plate, respectively.

The potential energy of blast loading can be calculated as

$$V = -W_d \int_0^\alpha P(t)r_p\phi(\theta)w_m(t)d\theta, \quad (34)$$

where $P(t)$ is applied blast pressure-time history and r_p is the radius at the outer layer of outer steel plate where blast loading is applied. Then, the equation of motion of curved SCS sandwich shell can be obtained by substituting Eqs. (26), (33), and (34) into Eq. (25). The fourth-order Runge-Kutta time stepping procedure was employed to solve the equation of motion and obtain the maximum mid-span displacement of curved SCS sandwich shell.

4 P-I diagram for curved SCS sandwich shell

Figure 15 shows the primary features of a P-I diagram and the pressure and impulse asymptotes are two vital parameters that define the limiting values for pressure and impulse, respectively. As seen in Fig. 15, the response behavior of a structure subjected to blast loading can be categorized into impulsive, dynamic, and quasi-static response regimes in accordance with the ratio of blast load duration to the natural period of the structure. The pressure and impulse asymptotes (quasi-static and impulsive response regimes) can be determined via employing the energy balance method and the responses in the dynamic response regime can be obtained by utilizing the SDOF method described in Section 3.

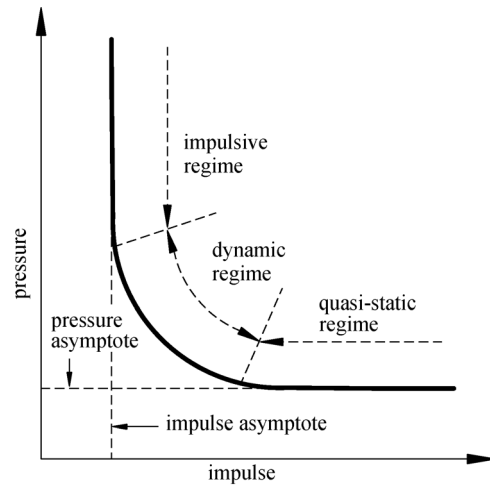


Fig. 15 Typical P-I diagram.

4.1 Internal energy-displacement relationship

The internal energy per unit width of concrete core can be calculated as

$$\bar{U}_c(w_m) = \bar{V}_c u_c, \quad (35)$$

where $\bar{V}_c = 1/2(r_{out}^2 - r_{in}^2)$ is the volume per unit width of concrete core and u_c is the internal energy per unit volume of concrete core, which can be calculated as

$$u_c(\varepsilon_c) = \int_0^{\varepsilon_c} \sigma_c d\varepsilon = \varepsilon_o f_{cm} \left[\frac{(k-1)^2 \varepsilon_c / \varepsilon_o - (\varepsilon_c / \varepsilon_o)^2}{(k-2)^2} - \frac{(k-1)^2 \ln\left(\frac{(k-2)\varepsilon_c / \varepsilon_o + 1}{(k-2)}\right)}{(k-2)^3} \right]. \quad (36)$$

Then, substituting $\varepsilon_c = \frac{w_m}{2R_c} - \frac{w_m^2\pi^2}{16R_c^2\alpha^2}$ into Eq. (36)

leads to the expression of internal energy per unit volume of concrete core in terms of mid-span displacement, $u_c(w_m)$. Similar to the calculation of internal energy per unit width of concrete core, $\bar{U}_c(w_m)$, the internal energy per unit width of inner and outer steel plate ($\bar{U}_{si}(w_m)$ and $\bar{U}_{so}(w_m)$) can be calculated as well. Herein, the relationship between internal energy per unit volume of steel plate and strain can be determined in Eq. (37) by adopting the elastic-plastic-hardening constitutive model in Eq. (32).

$$u_s(\varepsilon_s) = \int_0^{\varepsilon_s} \sigma_s d\varepsilon' = \begin{cases} 0.5E\varepsilon_s^2, & \varepsilon_s \leq \varepsilon_y, \\ 0.5\alpha_E E\varepsilon_s^2 + E(1-\alpha_E)(\varepsilon_y\varepsilon_s - 0.5\varepsilon_y^2), & \varepsilon_s > \varepsilon_y. \end{cases} \quad (37)$$

Then, the internal energy per unit width of curved SCS sandwich shell can be obtained by summing the internal energy contributed by concrete core, inner and outer steel plate as

$$\bar{U}(w_m) = \bar{U}_c(w_m) + \bar{U}_{si}(w_m) + \bar{U}_{so}(w_m), \quad (38)$$

where $\bar{U}_c(w_m)$, $\bar{U}_{si}(w_m)$, and $\bar{U}_{so}(w_m)$ are internal energy per unit width of concrete core, inner steel plate and outer steel plate, respectively.

4.2 Dimensionless pressure and impulse

The blast pressure profile is required when constructing the dimensionless P-I diagram. In this study, a triangular blast pressure profile with zero rise time given in Eq. (39) was adopted.

$$P(t) = \begin{cases} P_{\max}(1-t/t_d), & t < t_d \\ 0 & t \geq t_d \end{cases} \quad (39)$$

where P_{\max} is peak pressure and t_d is loading duration.

When loading duration is much longer than the natural period of curved SCS sandwich shell, i.e., $t_d \gg T$, the load can be considered to act in a quasi-static manner since the structure will reach its maximum displacement long before the load has diminished. Equating the external work done per unit width by blast loading with the internal energy per unit width of curved SCS sandwich shell leads to

$$\bar{U}(w_m) = \frac{1}{2}P_{\max}r_p w_m \alpha. \quad (40)$$

Then, rewriting Eq. (40) gives a modified pressure asymptote as

$$\frac{P_{\max}}{2\bar{U}(w_m)/r_p w_m \alpha} = 1 = \bar{P}, \quad (41)$$

where \bar{P} can be treated as the dimensionless pressure with the dimensionless pressure asymptote to be one.

When loading duration is much shorter than the natural period of curved SCS sandwich shell, i.e., $t_d \ll T$, the load can be considered to act in an impulsive manner. The blast energy initially transfers to the structure as kinetic energy and is finally absorbed by the structure as internal energy. Applying Momentum Theorem leads to

$$\frac{1}{4}P_{\max}r_p \alpha t_d = \frac{3}{8}\alpha \bar{m} \dot{w}_m, \quad (42)$$

where $\bar{m} = m/W_d$. The mid-span velocity of curved SCS sandwich shell, \dot{w}_m , can be determined from Eq. (42) and the velocity of the curved SCS shell, $\dot{w}(\theta)$, can also be obtained by applying the deflection shape function, $\phi(\theta)$. Then, the kinetic energy per unit width of curved SCS sandwich shell can be obtained as

$$\bar{E}_k = \frac{\alpha r_p^2 I^2}{3\bar{m}}, \quad (43)$$

where $I = 0.5P_{\max}t_d$ is impulse. Equating \bar{E}_k with $\bar{U}(w_m)$ gives the follow relationship:

$$\frac{\sqrt{\alpha} r_p I}{\sqrt{3\bar{m}\bar{U}(w_m)}} = 1 = \bar{I}, \quad (44)$$

where \bar{I} can be treated as the dimensionless impulse with the dimensionless impulse asymptote to be one.

4.3 Dimensionless P-I diagram construction

With the SDOF model described in Section 3 to obtain the maximum mid-span displacement of curved SCS sandwich shell under blast loading, the procedures to construct the dimensionless P-I diagram are described as follows:

1) Select the curved SCS sandwich shells with varying parameters, including geometry (angle α , radius, steel plate, and concrete core thickness), material (steel and concrete grade) and blast loading (peak pressure and loading duration). It should be noted that the adopted geometry of curved SCS sandwich shell must satisfy the geometry requirement specified in Section 3.

2) Obtain the maximum mid-span displacements of curved SCS sandwich shells with varying geometry, material and blast loading via employing the SDOF method and plot the pairs of dimensionless pressures, \bar{P} , and impulses, \bar{I} , in Fig. 16 (The dimensionless pressure and impulse are defined in Eqs. (41) and (44), respectively).

3) Fit the dimensionless pressure and impulse data in Fig. 16 and yield the formula of dimensionless P-I diagram in Eq. (45).

$$\ln(\bar{P}-1) + 0.039\ln^2(\bar{I}-1) + 0.864\ln(\bar{I}-1) + 1.288 = 0. \quad (45)$$

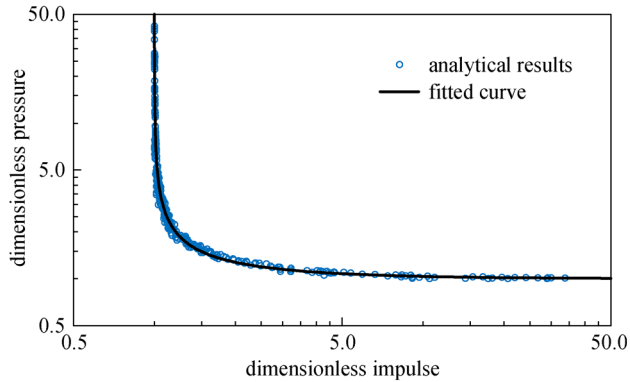


Fig. 16 Dimensionless P-I diagram from analytical model.

The dimensionless pressure, \bar{P} , and impulse, \bar{I} , in Eq. (45) are given in Eqs. (41) and (44), respectively, and they are functions of geometry and material properties of curved SCS sandwich shell, damage level (maximum displacement) as well as peak pressure and impulse of blast loading. Hence, the P-I diagram of a specific curved SCS sandwich shell can be directly plotted via Eq. (45) by inputting the geometry and material properties and allowable damage level of curved SCS sandwich shell. This convinces the easy application of the dimensionless P-I diagram and quick evaluation of the damage level of given curved SCS sandwich shell and blast loading. To validate the developed dimensionless P-I diagram, the established FE model in Section 2 was employed. Figure 17 compares the dimensionless pressures and impulses obtained from FE analyses with the analytically developed dimensionless P-I diagram. It is noted that the dimensionless P-I diagram constructed from SDOF method yields conservative prediction (i.e., higher damage level) as compared to those from the FE results. This is reasonable, since the FE model can capture the material's strain rate and confinement enhancement on concrete strength and these contribute to the blast resistant improvement of curved SCS sandwich shell. As compared in Fig. 18 for the compressive stress-strain curves from FE analyses and Eurocode 2, the initial slopes of the two models show good agreement. However, the ultimate strength and slopes near the ultimate strength of concrete from FE analyses are evidently higher as compared to Eurocode 2 due to the strain rate and confinement enhancement. These effects are nearly impossible to be included into the analytical model. In addition, the consistent compressive stress-strain curve distribution along the span of the curved SCS sandwich shell indicates the reasonable assumption that the strain was uniformly distributed along the curved SCS sandwich shell in Section 3.2.

Although some difference between FE and analytical predictions is observed, the developed dimensionless P-I diagram is easy to apply and can yield conservative predictions as compared to detailed FE analysis. In view of

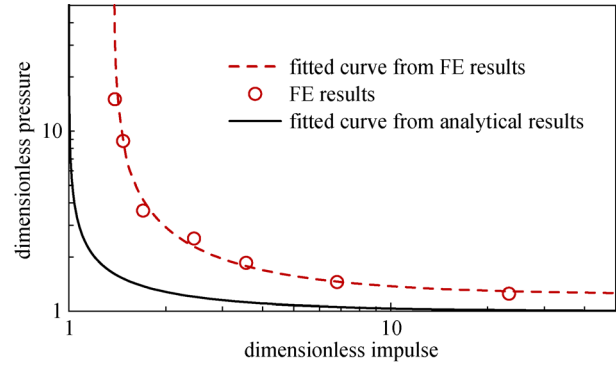


Fig. 17 Modified dimensionless P-I diagram with FE analyses.

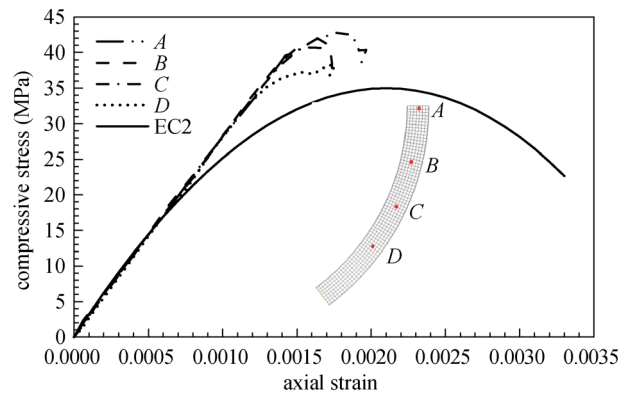


Fig. 18 Comparison of stress–strain curves from FE analyses and EC2.

the absence of analytical model for the curved SCS sandwich shell under blast loading, the developed dimensionless P-I diagram can be used to a convenient tool to quickly conduct the blast resistant design of such structures prior to detailed FE modeling.

5 Design approach

The procedures of using the constructed dimensionless P-I diagram to conduct the blast resistant design of curved SCS sandwich shell are presented as follows:

- 1) Determine the peak pressure and loading duration of a given blast loading;
- 2) Determine the maximum mid-span displacement based on the allowable damage level;
- 3) Choose the geometry and material properties of curved SCS sandwich shell and the selected geometry must satisfy the requirement specified in Section 3.
- 4) Calculate the dimensionless pressure and impulse from Eqs. (41) and (44), respectively, with the specified geometry and material properties, maximum mid-span displacement, peak pressure and loading duration from steps 1–3;

5) Check the location of dimensionless pressure and impulse with dimensionless P-I diagram plotted from Eq. (45). If the data point locates below the curve, the curved SCS sandwich shell experiences lower damage than the allowable damage level. Otherwise, the curved SCS sandwich shell experiences higher damage than the allowable damage level and it is needed to change the material or geometry properties of curved SCS sandwich shell and repeat the steps 3–5.

Since the ductility of concrete is much lower as compared to steel and the concrete core with larger volume is the main component to resist blast loading, two damage levels of curved SCS sandwich shell subjected to blast loading are suggested based on the compressive strain of concrete, i.e., $\varepsilon_{\max} = \varepsilon_o$ (damage level I) and ε_u (damage level II), where ε_o and ε_u are strain at peak stress and ultimate strain of concrete, respectively, and their values can be found from Eurocode 2 with specified concrete grade.

To simplify the calculation of internal energy as well as the formula of dimensionless P-I diagram, the assumption on axial strain is made and the corresponding geometry requirement of curved SCS sandwich shell to bring down the induced error is presented in Section 3. Herein, the procedures to select the suitable geometry of curved SCS sandwich shell are illustrated in Fig. 19 and described as follows:

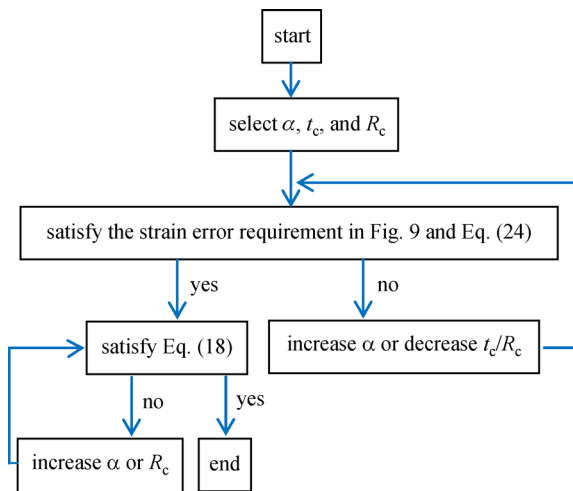


Fig. 19 Flow chart for determining the geometry of curved SCS sandwich shell.

1) Determine the concrete core thickness, t_c , radius, R_c , and angle α .

2) Check the strain error allowance by utilizing Fig. 12 and check the ratio of thickness to radius, t_c/R_c , with the allowable value in Eq. (24). If any of them is not satisfied, it is needed to increase α or decrease t_c/R_c and redo the checking.

3) Check the geometry parameters with Eq. (18). If not

satisfied, it is needed to increase α or R_c and redo the checking at current step.

6 Conclusions

The curved SCS sandwich shell was recently proposed to resist blast loading. In this paper, a dimensionless P-I diagram of curved SCS sandwich shell under blast loading was constructed based on energy balance and SDOF method to facilitate the blast resistant design of such structure. The main findings from this work are summarized as follows:

1) The equation of motion of the curved SCS sandwich shell was successfully established via employing the Lagrange's equation.

2) The pressure and impulse asymptotes could be obtained by utilizing the energy balance method, based on which, the dimensionless pressure and impulse were also defined.

3) The constructed dimensionless P-I diagram based on SDOF method yielded higher damage as compared to FE results, which might be due to the increased strength of concrete induced by strain rate and confinement effect.

4) This paper proposed the blast resistant design procedures of curved SCS sandwich shell utilizing the dimensionless P-I diagram, which could facilitate the blast resistant design of such structures.

Acknowledgements The research presented in this paper was financially supported by the National Natural Science Foundation of China (Grant No. 51608151), the China Postdoctoral Science Foundation (Nos. 2017T100245, 2016M600252), Heilongjiang Postdoctoral Fund (No. LBH-Z16063) and the Fundamental Research Funds for the Central Universities (No. HIT.NSRIF.2019069).

References

1. Oduyemi T O S, Wright H D. An experimental investigation into the behavior of double skin sandwich beams. *Journal of Constructional Steel Research*, 1989, 14(3): 197–220
2. Malek N, Machida A, Mutsuyoshi H, Makabe T. Steel-concrete sandwich members without shear reinforcement. *Transactions of the Japan Concrete Institute*, 1993, 15(2): 1279–1284
3. Foundoukos N. Behavior and design of steel-concrete-steel sandwich construction. Thesis for the Doctoral Degree. London: University of London, 2005
4. Huang Z, Liew J Y R. Structural behaviour of steel-concrete-steel sandwich composite wall subjected to compression and end moment. *Thin-walled Structures*, 2016, 98: 592–606
5. Yan J B, Liew J Y R, Zhang M H. Tensile resistance of J-hook connectors used in Steel-Concrete-Steel sandwich structure. *Journal of Constructional Steel Research*, 2014, 100: 146–162
6. Liew J Y R, Sohel K M A, Koh C G. Impact tests on steel-concrete-

- steel sandwich beams with lightweight concrete core. *Engineering Structures*, 2009, 31(9): 2045–2059
7. Remennikov A M, Kong S Y. Numerical simulation and validation of impact response of axially-restrained steel-concrete-steel sandwich panels. *Composite Structures*, 2012, 94(12): 3546–3555
 8. Anandavalli N, Lakshmanan N, Rajasankar J, Parkash A. Numerical studies on blast loaded steel-concrete composite panels. *JCES*, 2012, 1(3): 102–108
 9. Wang Y, Liew J Y R, Lee S C. Theoretical models for axially restrained steel-concrete-steel sandwich panels under blast loading. *International Journal of Impact Engineering*, 2015, 76: 221–231
 10. Crawford J E, Lan S. Blast barrier design and testing. In: *Proceedings of the ASCE Structures Congress*, St. Louis, Missouri, 2006
 11. Liew J Y R, Wang T Y. Novel steel-concrete-steel sandwich composite plates subjected to impact and blast load. *Advances in Structural Engineering*, 2011, 14(4): 673–687
 12. Lan S, Lok T S, Heng L. Composite structural panels subjected to explosive loading. *Construction & Building Materials*, 2005, 19(5): 387–395
 13. Wang Y, Liew J Y R, Lee S C. Experimental and numerical studies of non-composite Steel-Concrete-Steel sandwich panels under impulsive loading. *Materials & Design*, 2015, 81: 104–112
 14. Wang Y, Zhai X, Lee S C, Wang W. Responses of curved steel-concrete-steel sandwich shells subjected to blast loading. *Thin-walled Structures*, 2016, 108: 185–192
 15. Yan J B, Liew J Y R, Zhang M H, Soheli K M A. Experimental and analytical study on ultimate strength behavior of steel-concrete-steel sandwich composite beam structures. *Materials and Structures*, 2015, 48(5): 1523–1544
 16. Yan J B, Liew J Y R, Zhang M H, Li Z X. Punching shear resistance of steel-concrete-steel sandwich composite shell structure. *Engineering Structures*, 2016, 117: 470–485
 17. Yan J B, Xiong M X, Qian X, Liew J Y R. Numerical and parametric study of curved steel-concrete-steel sandwich composite beams under concentrated loading. *Materials and Structures*, 2016, 49(10): 3981–4001
 18. Yan J B, Richard Liew J Y, Qian X, Wang J Y. Ultimate strength behavior of curved Steel-Concrete-Steel sandwich composite beams. *Journal of Constructional Steel Research*, 2015, 115: 316–328
 19. Huang Z, Liew J Y R. Nonlinear finite element modeling and parametric study of curved steel-concrete-steel double skin composite panels infilled with ultra-lightweight cement composite. *Construction & Building Materials*, 2015, 95: 922–938
 20. Huang Z Y, Wang J Y, Richard Liew J Y, William Marshall P. Lightweight steel-concrete-steel sandwich composite shell subject to punching shear. *Ocean Engineering*, 2015, 102: 146–161
 21. Biggs J M. *Introduction to Structural Dynamics*. New York: McGraw-Hill, 1964
 22. Wang Y, Xiong M X. Analysis of axially restrained water storage tank under blast loading. *International Journal of Impact Engineering*, 2015, 86: 167–178
 23. Rigby S E, Tyas A, Bennett T. Elastic-plastic response of plates subjected to cleared blast loads. *International Journal of Impact Engineering*, 2014, 66: 37–47
 24. Morison C M. Dynamic response of walls and slabs by single-degree-of-freedom analysis—a critical review and revision. *International Journal of Impact Engineering*, 2006, 32(8): 1214–1247
 25. Nassr A A, Razaqpur A G, Tait M J, Campidelli M, Foo S. Single and multi degree of freedom analysis of steel beams under blast loading. *Nuclear Engineering and Design*, 2012, 242(1): 63–77
 26. Carta G, Stochino F. Theoretical models to predict the flexural failure of reinforced concrete beams under blast loads. *Engineering Structures*, 2013, 49: 306–315
 27. Krauthammer T, Bazeos N, Holmquist T J. Modified SDOF analysis of box-type structures. *Journal of Structural Engineering*, 1986, 112(4): 726–744
 28. Astarlioglu S, Krauthammer T, Morency D, Tran T P. Behavior of reinforced concrete columns under combined effects of axial and blast-induced transverse loads. *Engineering Structures*, 2013, 55: 26–34
 29. UFC 3-340-02. *Structures to Resist the Effects of Accidental Explosions*. Washington, D.C.: US Department of Army, Navy and the Air Force, 2008
 30. ASCE. *Design of Blast-Resistant Buildings in Petrochemical Facilities*. American Society of Civil Engineers, 2010
 31. ASCE. *Blast Protection of Buildings*. ASCE/SEI 59-11. American Society of Civil Engineers, 2011
 32. Mays G, Smith P D. *Blast Effects on Buildings: Design of Buildings to Optimize Resistance to Blast Loading*. London: T. Telford, 1995
 33. Li Q M, Meng H. Pressure-impulse diagram for blast loads based on dimensional analysis and single-degree-of-freedom mode. *Journal of Engineering Mechanics*, 2002, 128(1): 87–92
 34. Li Q M, Meng H. Pulse loading shape effects on pressure-impulse diagram of an elastic-plastic, single-degree-of-freedom structural model. *International Journal of Mechanical Sciences*, 2002, 44(9): 1985–1998
 35. Fallah A S, Louca L A. Pressure-impulse diagrams for elastic-plastic-hardening and softening single-degree-of-freedom models subjected to blast loading. *International Journal of Impact Engineering*, 2007, 34(4): 823–842
 36. Krauthammer T, Astarlioglu S, Blasko J, Soh T B, Ng P H. Pressure-impulse diagrams for the behaviour assessment of structural components. *International Journal of Impact Engineering*, 2008, 35(8): 771–783
 37. Dragos J, Wu C. A new general approach to derive normalised pressure impulse curves. *International Journal of Impact Engineering*, 2013, 62: 1–12
 38. Shi Y, Hao H, Li Z X. Numerical derivation of pressure-impulse diagrams for prediction of RC column damage to blast loads. *International Journal of Impact Engineering*, 2008, 35(11): 1213–1227
 39. Mutalib A A, Hao H. Development of P-I diagrams for FRP strengthened RC columns. *International Journal of Impact Engineering*, 2011, 38(5): 290–304
 40. Rabczuk T, Areias P M A, Belytschko T. A meshfree thin shell method for non-linear dynamic fracture. *International Journal for Numerical Methods in Engineering*, 2007, 72(5): 524–548
 41. Nguyen-Thanh N, Zhou K, Zhuang X, Areias P, Nguyen-Xuan H, Bazilevs Y, Rabczuk T. Isogeometric analysis of large-deformation

- thin shells using RHT-splines for multiple-patch coupling. *Computer Methods in Applied Mechanics and Engineering*, 2017, 316: 1157–1178
42. Rabczuk T, Kim J Y, Samaniego E, Belytschko T. Homogenization of sandwich structures. *International Journal for Numerical Methods in Engineering*, 2004, 61(7): 1009–1027
 43. Rabczuk T, Zi G, Bordas S, Nguyen-Xuan H. A geometrically non-linear three-dimensional cohesive crack method for reinforced concrete structures. *Engineering Fracture Mechanics*, 2008, 75(16): 4740–4758
 44. Rabczuk T, Zi G, Bordas S, Nguyen-Xuan H. A simple and robust three-dimensional cracking-particle method without enrichment. *Computer Methods in Applied Mechanics and Engineering*, 2010, 199(37–40): 2437–2455
 45. Rabczuk T, Belytschko T. A three-dimensional large deformation meshfree method for arbitrary evolving cracks. *Computer Methods in Applied Mechanics and Engineering*, 2007, 196(29–30): 2777–2799
 46. Hallquist J O. *LS-DYNA Theory Manual*. Livermore Software Technology Corporation (LSTC), 2006
 47. Foundoukos N, Chapman J C. Finite element analysis of steel-concrete-steel sandwich beams. *Journal of Constructional Steel Research*, 2008, 64(9): 947–961
 48. Clubleby S K, Moy S S J, Xiao R Y. Shear strength of steel-concrete-steel composite panels. Part II—Detailed numerical modelling of performance. *Journal of Constructional Steel Research*, 2003, 59(6): 795–808
 49. Li X, Chen J F, Lu Y, Yang Z. Modelling static and dynamic FRP-concrete bond behaviour using a local concrete damage model. *Advances in Structural Engineering*, 2015, 18(1): 45–58
 50. Chen W, Hao H, Chen S. Numerical analysis of prestressed reinforced concrete beam subjected to blast loading. *Materials & Design*, 2015, 65: 662–674
 51. Federal Highway Administration. *Users Manual for LS-DYNA Concrete Material Model 159*. Publication No. FHWA-HRT-05-062, 2007
 52. Federal Highway Administration. *Evaluation of LS-DYNA Concrete Material Model 159*. Publication No. FHWA-HRT-05-063, 2007
 53. Cowper G R, Symonds P S. *Strain Hardening and Strain Rate Effects in the Impact Loading of Cantilever Beams*. Applied Mathematics Report. 1958
 54. Jones N. *Structural Impact*. Cambridge/New York: Cambridge University Press, 1988
 55. Kang W K, Lee S C, Liew J Y R. Analysis of steel-concrete composite column subject to blast. *Proceedings of the Institution of Civil Engineers. Structures and Buildings*, 2013, 166(1): 15–27
 56. Xie M, Foundoukos N, Chapman J C. Static tests on steel-concrete-steel sandwich beams. *Journal of Constructional Steel Research*, 2007, 63(6): 735–750
 57. Dym C L, Williams H E. Stress and displacement estimates for arches. *Journal of Structural Engineering*, 2011, 137(1): 49–58
 58. Baker W E, Cox P A, Westine P S, Kulesz J J, Strehlow R A. *Explosion and Hazards and Evaluation*. Amsterdam: Elsevier Scientific Publishing Company, 1983
 59. Eurocode 2. *Design of concrete structures—part 1-1: General Rules and Rules for Buildings*. EN 1992-1-1. London: British Standards Institution, 2004